# Polarization-Dependent Multi-Functional Metamaterial as Polarization Filter, Transparent Wall and Circular Polarizer using Ring-Cross Resonator

*Zhao ZHANG [1], Xiangyu CAO [1], Jun GAO [1], Sijia LI [1], Liming XU [2]*

[1]Information and Navigation College, Air Force Engineering University, Xi'an 710077, China
[2]Science and Technology on Electronic Information Control Laboratory, Chengdu 610036, China

bjzhangzhao323@126.com, xiangyucaokdy@163.com, gjgj9694@163.com, lsj051@126.com, 10575229@qq.com

Submitted July 5, 2016 / Accepted November 6, 2016

**Abstract.** *We propose a polarization-dependent multi-functional metamaterial using ring-cross resonator. Based on the analysis of surface current distributions induced by different polarized incidence, we demonstrate that the proposed metamaterial serves as a polarization filter, a transparent wall and a circular polarizer under different polarization normal incidence. Additionally, parameter analyses on the control of resonance are discussed to complementally explain the physical origin. Simulated results show that the proposed metamaterial functions as a polarization filter eliminating the x-polarization wave at 10.1 GHz and y-polarization wave at 14.3 GHz, a transparent wall transmitting both x-polarized and y-polarized incident waves at 12.6 GHz, and a broadband circular polarizer converting the +45° polarized (–45° polarized) incident wave to the left (right) handed circularly polarized wave from 10.8 to 12.8 GHz, respectively. Measured results agree well with the simulation and validate the performance of the proposed multifunctional metamaterial.*

## Keywords

Metamaterial, polarization filter, circular polarizer

## 1. Introduction

During the past decades, many fascinating functional metamaterials have been developed, such as invisible cloak [1], perfect absorbers [2–5], and high impedance surfaces [6–8]. Till now, it's still one of research interests to control electromagnetic wave utilizing metamaterials [9–12]. Polarization plays an important role among all the properties of electromagnetic wave, and great efforts have been made to design polarization-independent and polarization-dependent metamaterials. Polarization-independent metamaterials have the advantage that they exhibit good performance whatever the polarization state is. For example, polarization-independent perfect absorbers have good absorption for both TE and TM incident waves [13–17]. However, polarization-dependent metamaterials exhibit different performance under different polarization incidence. Based on this concept, anisotropic or chiral metamaterials have been extensively investigated in terms of asymmetric transmission [18–21], circular polarizer [22–25] and negative refractive index [26–28]. What's more, metamaterials with multiple functionalities is also a research focus [29] and the multiple functionalities can be controlled by the polarization state of incident wave [30].

In this work, we proposed a polarization-dependent multi-functional metamaterial (PDMFM) using ring-cross resonator. The resonator consists of a ring and a centrally placed cross with unequal length of arms. From the surface current distributions and parameter analyses, we theoretically demonstrate that the PDMFM has different functions under different polarization incidence. At 10.1 GHz and 14.3 GHz, the PDMFM functions as a polarization filter which eliminates *x*-polarized wave and *y*-polarized wave, respectively. At 12.6 GHz, the PDMFM functions as a transparent wall which transmits both *x*-polarized and *y*-polarized wave. From 10.8 to 12.8 GHz, the PDMFM functions as a broadband circular polarizer which converts the +45° polarized (–45° polarized) incident wave to the left (right) handed circularly polarized wave. As a circular polarizer, the refraction bandwidth of axis ratio (AR) lower than 3 dB reaches 16.95%. To verify the above polarization-dependent multiple functionalities experimentally, we fabricated and measured the PDMFM sample. The good agreement between simulation and measurement validates the good performance.

## 2. Design and Analysis

Figure 1 shows the unit cell of the proposed PDMFM which is composed of two layers of planar ring-cross resonators etched on the two sides of a dielectric substrate with thickness of $h$, relative permittivity of $\varepsilon_r = 2.2$ and loss tangent of 0.0009. The ring-cross resonator consists of a ring and a centrally placed cross with two arms of unequal length, pointing towards *x*-axis and *y*-axis, respec-

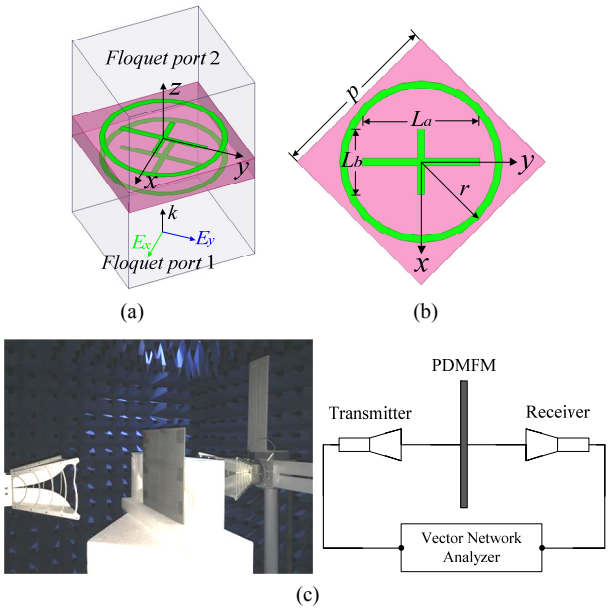


**Fig. 1.** Geometry of the PDMFM. (a) Simulation model. (b) Top view. (c) Measurement setup.

tively. The two layers of resonators have the same dimension and the coincident projection on the *x*-*o*-*y* plane. The other parameters include the structure periodic $p$, the radius $r$, and the unequal arm lengths $L_a$ and $L_b$. The optimized geometrical parameters are as follows: $p$ =11.5 mm, $L_a$ = 7.7 mm, $L_b$ = 4.4 mm, $r$ = 5.4 mm and $h$ = 4 mm.

To analyze the performance of the PDMFM, the numerical simulation is performed using Ansoft HFSS. The periodical boundary conditions are adopted, and two Floquet ports are assigned on the top and bottom boundary along $z$ direction. The plane wave with linear polarization along $x$ or $y$ direction normally illuminates on the sample along $z$ direction. Under the Cartesian coordinate system, the transmitted waves $E^t_x$ and $E^t_y$ associate with the incident waves $E^i_x$ and $E^i_y$ through the transmission matrix $\mathbf{T}_l$ as follows: [23], [24]

$$\begin{pmatrix} E^t_x \\ E^t_y \end{pmatrix} = \mathbf{T}_l \begin{pmatrix} E^i_x \\ E^i_y \end{pmatrix} = \begin{bmatrix} t_{xx} & t_{xy} \\ t_{yx} & t_{yy} \end{bmatrix} \begin{pmatrix} E^i_x \\ E^i_y \end{pmatrix} \tag{1}$$

where $t_{uv}$ means the transmission coefficient between the transmitted $u$-polarized wave and the incident $v$-polarized wave. For the circular polarization, the transmitted left handed polarized wave $E^t_+$ and right handed polarized wave $E^t_-$ can be written as:

$$\begin{pmatrix} E^t_+ \\ E^t_- \end{pmatrix} = \frac{1}{\sqrt{2}} \begin{pmatrix} E^t_x + \mathrm{j}E^t_y \\ E^t_x - \mathrm{j}E^t_y \end{pmatrix} = \mathbf{T}_c \begin{pmatrix} E^i_x \\ E^i_y \end{pmatrix}, \tag{2}$$

$$\mathbf{T}_c = \begin{pmatrix} T_{+x} & T_{+y} \\ T_{-x} & T_{-y} \end{pmatrix} = \frac{1}{\sqrt{2}} \begin{bmatrix} t_{xx} + \mathrm{j}t_{yx} & t_{xy} + \mathrm{j}t_{yy} \\ t_{xx} - \mathrm{j}t_{yx} & t_{xy} - \mathrm{j}t_{yy} \end{bmatrix}. \tag{3}$$

Then the mechanism of multiple functionalities can be demonstrated according to the transmission matrix. As shown in Fig. 2, for a polarization filter which transmits *y*-

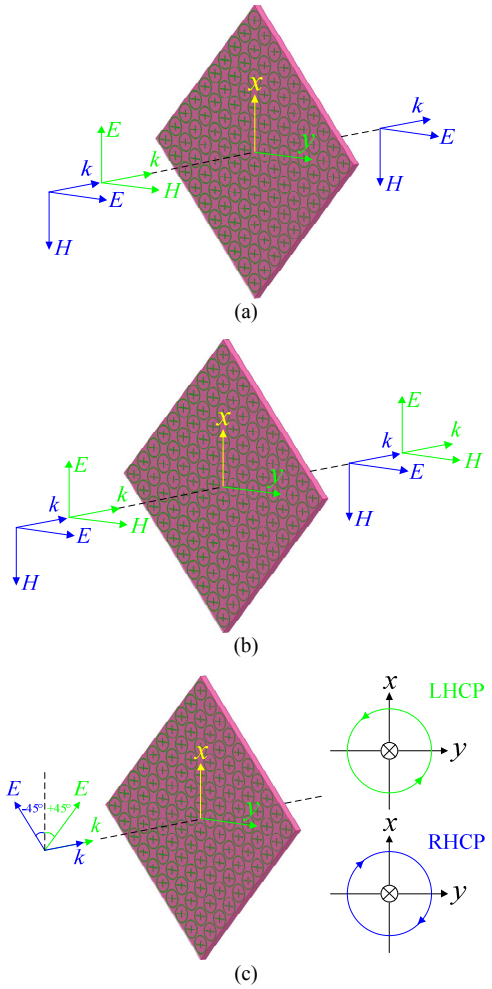


**Fig. 2.** The PDMFM serves as a polarization filter, transparent wall, and polarization converter. (a) Polarization filter eliminating *x*-polarized incident wave. (b) Transparent wall transmitting both *x*-polarized and *y*-polarized incident wave. (c) Circular polarizer converting the +45° (–45°) polarized incident wave to left handed (right handed) circularly polarized wave.

polarized (*x*-polarized) wave but eliminates *x*-polarized (*y*-polarized) wave, equation (1) indicates that the amplitude of $t_{yy}$ ($t_{xx}$) is close to 1 while $t_{xy}$, $t_{yx}$ and $t_{xx}$ ($t_{yy}$) should be much smaller than $t_{yy}$ ($t_{xx}$). For a transparent wall which transmits both *x*-polarized and *y*-polarized wave, equation (1) indicates that both $t_{xx}$ and $t_{yy}$ are close to 1 while $t_{xy}$ and $t_{yx}$ should be much smaller than $t_{xx}$ and $t_{yy}$. For a circular polarizer which converts the incident ±45° polarized wave into the transmitted circularly polarized wave, equation (3) indicates that the amplitudes of $t_{xx}$ and $t_{yy}$ should be equal to each other and much larger than $t_{yx}$ and $t_{xy}$, and the phase difference $\Delta\theta$ between $t_{yy}$ and $t_{xx}$ should be equal to ±90°. In a word, the transmission matrix which has the specific element value varying with frequency leads to the multiple functionalities.

To verify the theoretical analysis, the proposed PDMFM has been fabricated and measured in a microwave anechoic chamber as shown in Fig. 1(c). The fabricated sample consists of 26 × 26 unit cells with a total square area of 299 mm × 299 mm. A vector network analyzer

(Agilent N5230C) and two broadband linearly polarized horn antennas with a distance of 1 m to each other were used to constitute the test system. The sample was placed in the middle between the horn antennas. The time-domain gating strategy was used to eliminate the undesirable wave. The co-polarization transmission coefficients ($t_{xx}$ and $t_{yy}$) and cross-polarization transmission coefficients ($t_{yx}$ and $t_{xy}$) were measured by rotating the receiving and transmitting horn antenna 0° and 90°, respectively. To measure the linear-to-circular polarization conversion, we changed the relative position of the sample to guarantee the ±45° polarized incidence.

## 3. Results and Discussion

Figure 3 shows the simulated and measured transmission coefficients for the *x*-polarization and *y*-polarization propagation along +*z* direction. The simulation and measurement results are in good agreement in the entire frequency range. It is observed that the cross-polarization transmission coefficients are as low as enough to be neglected. For the co-polarization transmission, both the amplitude and phase of $t_{xx}$ and $t_{yy}$ have different trends with frequency. Firstly, at 10.1 GHz, $t_{yy}$ is close to 0 dB while $t_{xx}$ is lower than –10 dB, which means that the *y*-polarized incident wave is transmitted while the *x*-polarized incident wave is eliminated. At 14.3 GHz, $t_{xx}$ is about –0.8 dB while $t_{yy}$ is lower than –40 dB, which means that the *x*-polarized incident wave is transmitted while the *y*-polarized incident wave is eliminated. Thus, the PDMFM functions as a polarization filter that filters out the *x*-polarized incidence at 10 GHz and the *y*-polarized incidence at 14.3 GHz, respectively. Secondly, at 12.6 GHz, both $t_{xx}$ and $t_{yy}$ are close to 0 dB, which means that both *x*-polarized and *y*-polarized incident waves are transmitted. Namely, the PDMFM functions as a transparent wall that is transparent for both *x*-polarized and *y*-polarized incidence at 12.6 GHz. Finally, from 11.5 to 13 GHz, $t_{xx}$ and $t_{yy}$ have the similar amplitudes but different phases. The phase difference $\Delta\theta$ is about +90° from 10.5 to 12.5 GHz. That's to say, under ±45° polarized incidence, the PDMFM functions as a circular polarizer that converts the incident linearly polarized wave to a transmitted circularly polarized wave.

To better understand the performance of the PDMFM as a circular polarizer, the ellipticity $\chi$ and polarization azimuth rotation angle $\tau$ of the transmitted wave are calculated using the following equations [31], [32]

$$\chi = \frac{1}{2}\arcsin\left(\frac{2a_x a_y}{a_x^2 + a_y^2}\sin(\Delta\varphi)\right), \tag{4}$$

$$\tau = \frac{1}{2}\arctan\left(\frac{2a_x a_y}{a_x^2 - a_y^2}\cos(\Delta\varphi)\right) \tag{5}$$

where $a_x$ and $a_y$ are the magnitudes of electric field components along *x*-axis and *y*-axis, and $\Delta\varphi = \arg(a_y) - \arg(a_x)$. The polarization azimuth rotation angle $\tau$ represents the

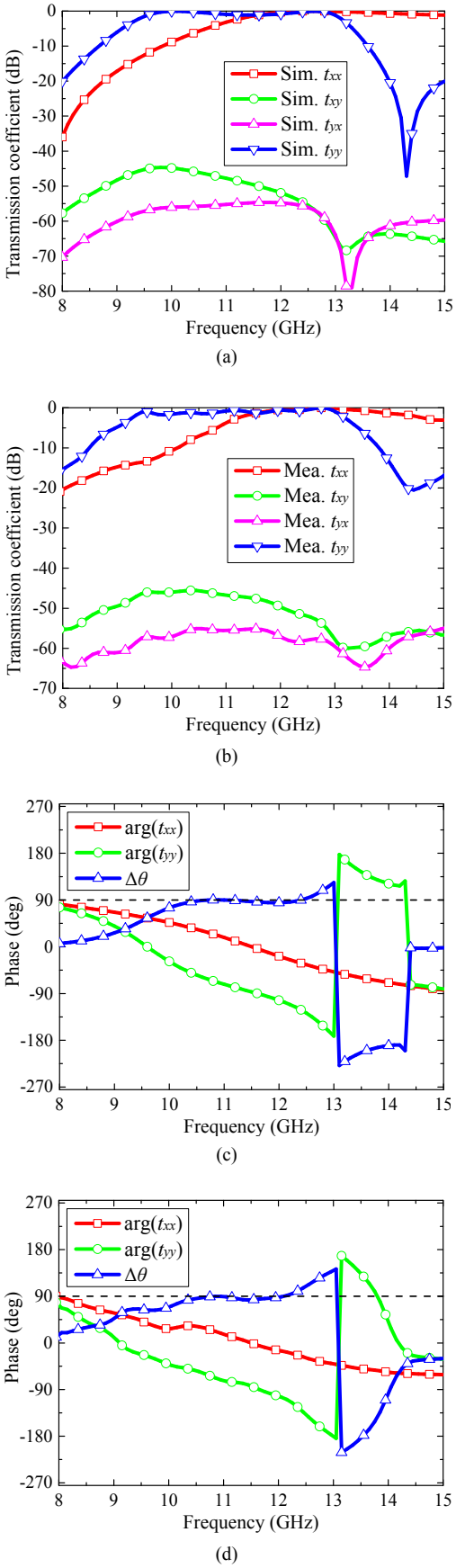


**Fig. 3.** Simulated and measured transmission coefficients for the propagation along +z direction. (a), (c) Simulated results. (b), (d) Measured results.

angle between the major axis of elliptical wave and $x$-axis. Then, the axis ratio can be calculated as

$$AR = \left| \frac{1}{\tan \chi} \right|. \quad (6)$$

For the circularly polarized wave, $\chi$ should be ±45°. If $\chi = +45°$, then $AR = 1$, which means the transmitted wave is a left handed circularly polarized wave. If $\chi = -45°$, then the transmitted wave is a right handed circularly polarized wave.

The corresponding numerical and experimental results for +45° polarization incidence are plotted in Fig. 4. From Fig. 4(a), we can see the ellipticity $\chi$ is close to +45° from 11.5 to 12.4 GHz, which indicates a left handed circularly polarized wave. What's more, the proposed PDMFM performs broadband linear-to-circular polarization conversion. Figure 4(c) shows that the bandwidth of $AR < 3$ dB covers the range from 10.8 to 12.8 GHz with a fraction bandwidth of 16.9%. To illustrate the polarization state of transmitted circularly polarized wave, the polarization ellipses at different frequencies are shown in Fig. 5. The direction of major axis is obtained from the ellipse polarization azimuth rotation angle $\tau$, as shown in Fig. 4(b). At 10.8 and 12.8 GHz, the upper and lower side frequency of the working band, the transmitted waves are left handed elliptical and the major axis of ellipse is tilted on –45.6° and 87.8° with respect to $x$-axis, respectively. At 11.5 and 12.4 GHz, $AR$ reaches minimal values close to 0 dB. So the transmitted waves are left handed circular and the major axis of ellipse is tilted on –13.8°and 52.6° with respect to $x$-axis, respectively. It should be pointed out that, whether the transmitted circularly polarized wave is left handed or right handed, is depend on the polarization state of the incident wave. Due to the symmetry in the structure, the transmitted wave will be a right handed circularly polarized wave if the incidence is changed to be –45° polarized.

To understand the physical mechanism of multiple functionalities, the induced surface current distributions on bottom and top layers under different polarization incidence at typical frequencies are depicted in Fig. 6.

As shown in Fig. 6(a), at 10.1 GHz, the currents on the bottom and top layer are in the same direction and the ring-cross resonator behaves as an electric dipole resonator. So both $x$-polarized and $y$-polarized incidences induce the electric dipole resonance. Under $x$-polarized incidence, the current on the bottom layer is strong, while the current on the top layer is weak, which generate a weak electric resonance between the bottom and top layer. Thus, $x$-polarized wave cannot be transmitted. However, under $y$-polarized incidence, the current on the top layer is strong, which generate a strong electric resonance. Then the $y$-polarized wave can be transmitted [33]. So the PDMFM functions as a polarization filter that filters out the $x$-polarized wave at 10.1 GHz.

As shown in Fig. 6(b), at 14.3 GHz, the $x$-polarized incidence induces the electric resonance and the current on

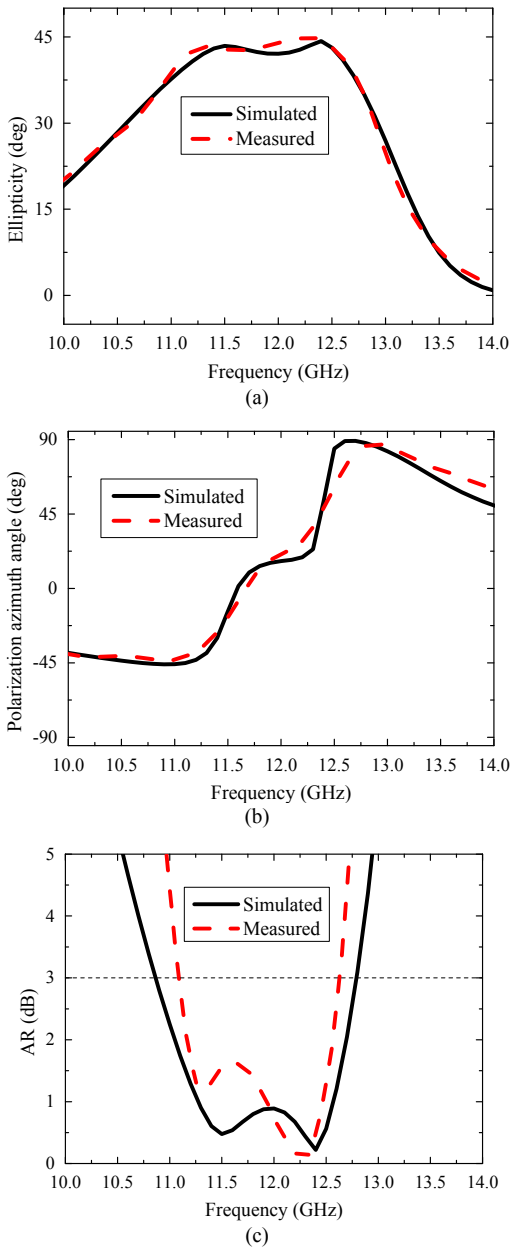


**Fig. 4.** Numerical and experimental results: (a) $\chi$, (b) $\tau$, (c) $AR$.

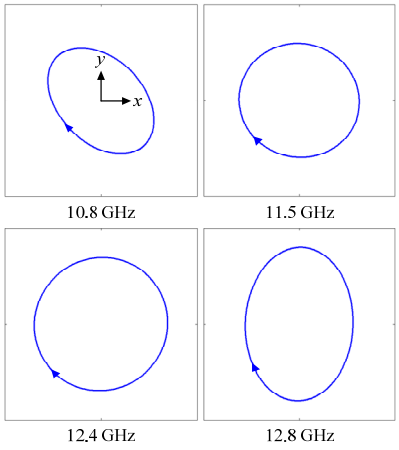


**Fig. 5.** Polarization ellipses (waves are coming out of the paper).

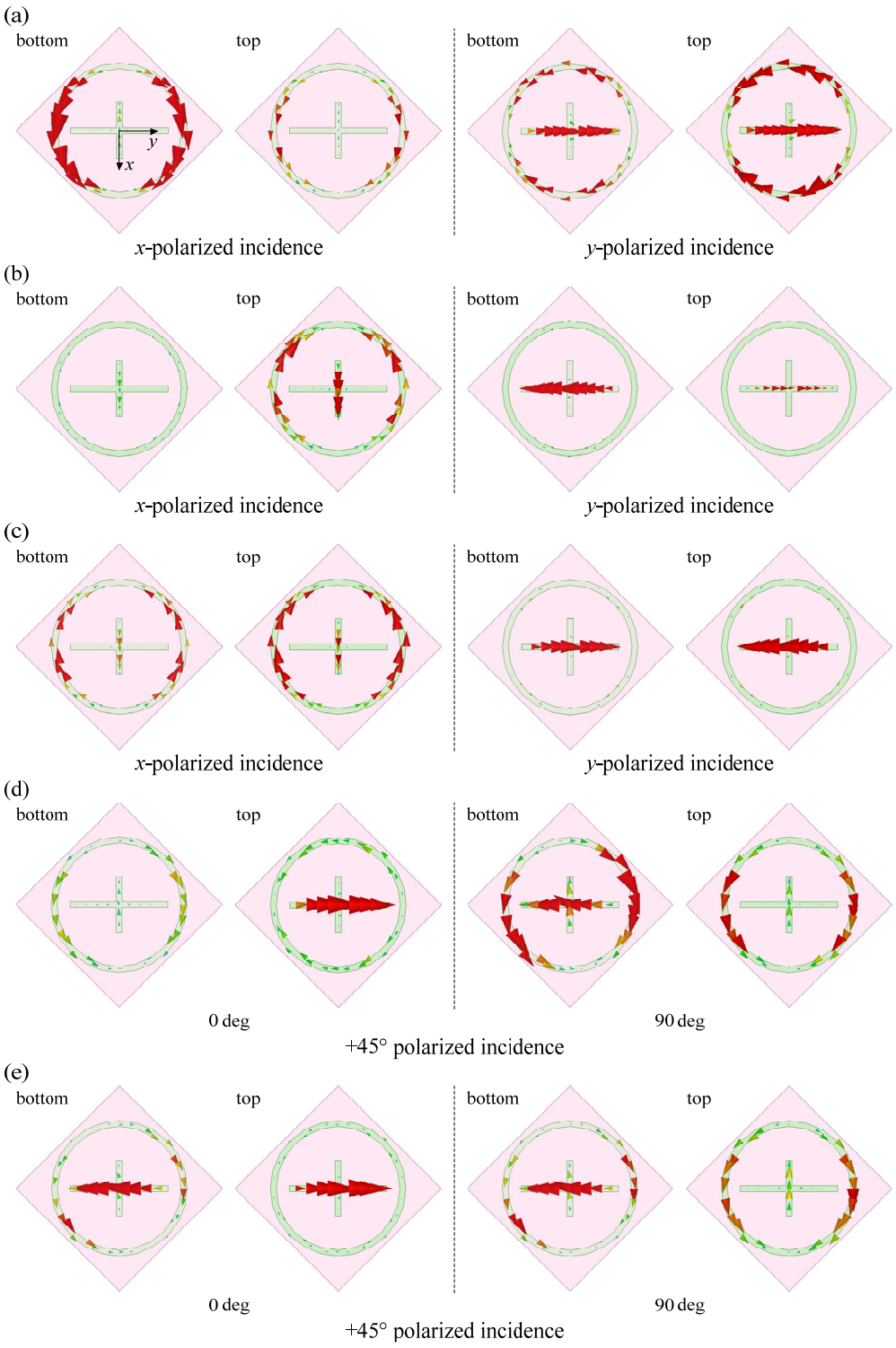


**Fig. 6.** The induced surface current distributions under different polarization incidence: (a) 10.1 GHz; (b) 14.3 GHz; (c) 12.6 GHz; (d) 11.5 GHz; (e) 12.4 GHz.

the top layer is strong. So the *x*-polarized incidence can be transmitted. Under *y*-polarized incidence, the induced currents on the bottom and top layers are in the opposite direction, which exhibits a magnetic response [34]. However the current on the top layer is weak and the magnetic response is also weak. Thus, the *y*-polarized wave cannot be transmitted. So the PDMFM functions as a polarization filter that filters out the *y*-polarized wave at 14.3 GHz.

As shown in Fig. 6(c), at 12.6 GHz, *x*-polarized incidence induces the strong electric resonance, while *y*-polarized incidence induces the strong magnetic response. So both *x*-polarized and *y*-polarized incident wave can be transmitted and the PDMFM functions as a transparent wall.

As shown in Fig. 6(d) and 6(e), at 11.5 and 12.4 GHz, the electric field of +45° polarized incident wave can be

decomposed into two components along *x*-axis and *y*-axis with the same amplitude. As a result, both electric resonance and magnetic resonance are induced. Meanwhile, the current direction on top layer follows the left handed rule with the phase changing. Thus, the PDMFM functions as a circular polarizer that converts the +45° polarized incident wave to the left handed circularly polarized wave.

In order to demonstrate the performance of the proposed PDMFM in the typical case of oblique incidence, Figure 7 shows the simulated transmission at incident angles from 0° to 60° under different polarized incidence. For both of the TE-polarized and TM-polarized incidence, the transmission coefficient shifts slowly toward lower frequency when the incident angle increases. As a polarization filter that filters out the TM-polarized wave, the resonant frequency shifts from 10.1 GHz to 9.6 GHz when the incident angle increase from 0° to 60°. Similarly, as a polarization filter that filters out the TE-polarized wave, the resonant frequency also shifts slowly toward lower frequency with the incident angle increasing. As a transparent wall, the resonant frequency almost keeps the same around 12.6 GHz with the incident angle increasing. From Fig. 7 we can see, compared with normal incidence, the oblique incidence leads to the slight frequency shift but this phenomenon has relatively little influence on the performance of the proposed PDMFM.

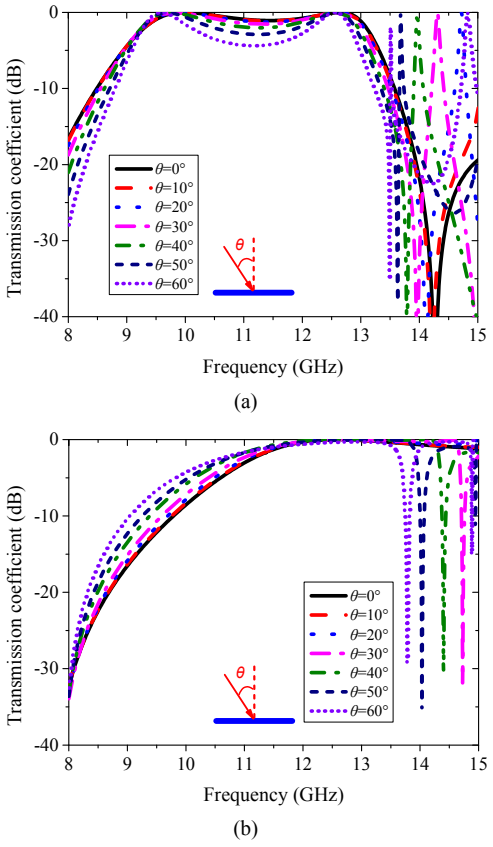


**Fig. 7.** Simulated transmission for the incident wave at incident angles from 0° to 60°. (a) TE-polarized incidence, and (b) TM-polarized incidence.

## 4. Control of Resonances

Finally, we demonstrate three parameter analyses for the independent control of resonances. Figure 8 and 9 depict the effects of cross arm length $L_a$ and $L_b$ on the transmission. From Fig. 8 we can see the transmission $t_{yy}$ shifts toward lower frequency when $L_a$ increases, while the transmission $t_{xx}$ almost keeps unchanged. On the other hand, Figure 8 shows that the transmission $t_{xx}$ shifts toward lower frequency when $L_b$ increases, while the transmission $t_{yy}$ almost keeps unchanged. Figure 10 depicts the effects of ring radius $r$ on the transmission. Different from the effects of cross arms, the ring has little influence on the resonant frequencies. Instead, it influences the variation trend of $t_{xx}$ and $t_{yy}$ in low frequency band. The above phenomenon indicates that the resonant frequency of $t_{yy}$ is decided by the length $L_a$ while the resonant frequency of $t_{xx}$ is decided by the length $L_b$. The physical origin is explained by the resonant mode of the ring-cross structure. From Fig. 6 we conclude that the ring-cross structure behaves as electric dipole resonators under *x*-polarized or *y*-polarized incidence. That is to say, the length $L_a$ and $L_b$ decide the resonant frequency of the equivalent electric dipole resonators along *y*-axis and *x*-axis, independently. Then the anisotropy along *y*-axis and *x*-axis determines the different transmission amplitude and phase, and different polarization-dependent functionalities are realized.

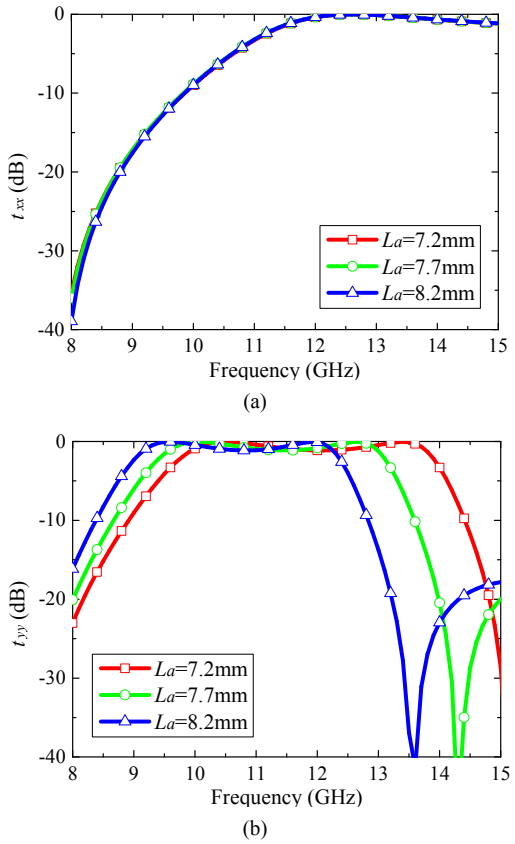


**Fig. 8.** Effects of cross arm length $L_a$ on the transmission. (a) $t_{xx}$, and (b) $t_{yy}$.

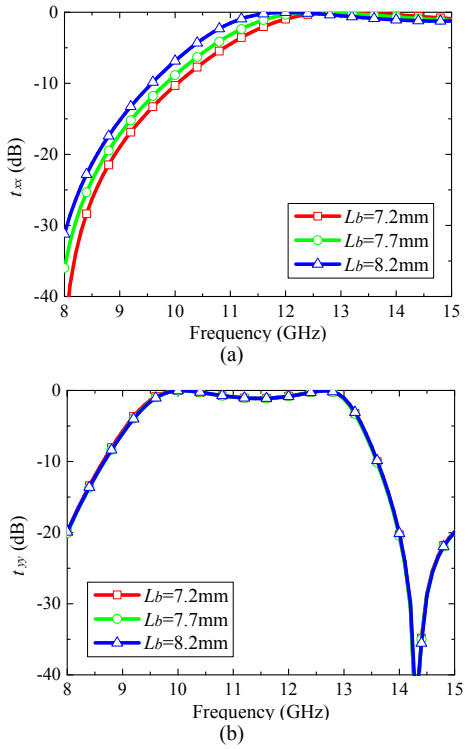


**Fig. 9.** Effects of cross arm length $L_b$ on the transmission (a) $t_{xx}$, and (b) $t_{yy}$.

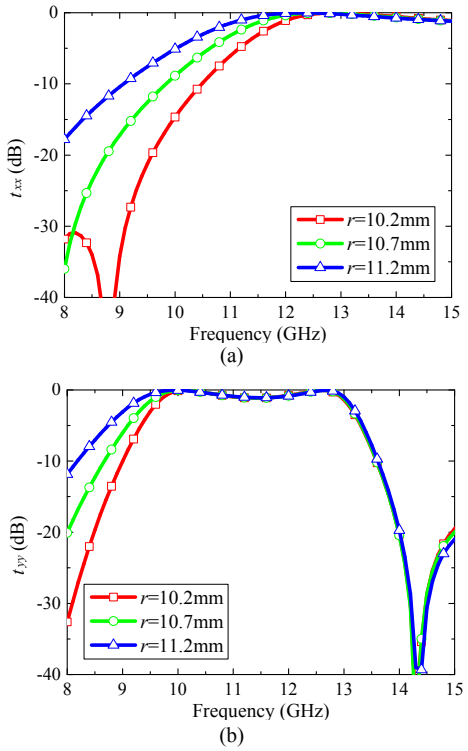


**Fig. 10.** Effects of ring radius $r$ on the transmission (a) $t_{xx}$, and (b) $t_{yy}$.

## 5. Conclusion

In conclusion, we have proposed a polarization-dependent multi-functional metamaterial using the ring-cross resonator. From the analyses on transmission matrix and surface current distribution, we theoretically demonstrate that the PDMFM functions as a polarization filter, transparent wall and circular polarizer under normal incidence with different polarizations. Meanwhile, as a circular polarizer, the PDMFM has a broad refraction bandwidth of 16.9% for $AR < 3$ dB. To verify the theoretical analyses and simulation, the PDMFM has been fabricated and measured. The good agreement between simulation and measurement validates the performance of the PDMFM.

## Acknowledgments

This work is supported by the National Natural Science Foundation of China (No. 61271100, No. 61471389 and No. 61671464) and the Natural Science Foundational Research Fund of Shaanxi Province (No. 2017JM6025). Authors also thank reviewers for their valuable comments.

## References

[1] MEI, Z., NIU, T., BAI, J., CUI, T. Design of transparent cloaks with arbitrarily inner and outer boundaries. *Journal of Applied Physics*, 2010, vol. 107, no. 12, p. 124908-(1–6). DOI: 10.1063/1.3452389

[2] LIU, T., CAO, X., GAO, J., et al. RCS reduction of waveguide slot antenna with metamaterial absorber. *IEEE Transactions on Antennas and Propagation*, 2013, vol. 61, no. 3, p. 2327–2335. DOI: 10.11 09/TAP.2012.2231922

[3] LI, S. J., GAO, J., CAO, X. Y., ZHANG, Z. Loaded metamaterial perfect absorber using substrate integrated cavity. *Journal of Applied Physics*, 2014, vol. 115, no. 21, p. 213703-(1–5). DOI: 10.1063/1.4881115

[4] ZHU, B., FENG, Y., ZHAO, J., et al. Polarization modulation by tunable electromagnetic metamaterial reflector/absorber. *Optics Express*, 2010, vol. 18, p. 023196–203. DOI:10.1364/OE.18.023196

[5] LI, S. J., GAO, J., CAO, X. Y., et al. Hybrid metamaterial device with wideband absorption and multiband transmission based on spoof surface plasmon polaritons and perfect absorber. *Applied Physics Letters*, 2015, vol. 106, no. 18, p. 181103-(1–5). DOI: 10.1063/1.4919789

[6] CHEN, X., LI, L., LIANG, C., et al. Dual-band high impedance surface with mushroom-type cells loaded by symmetric meandered slots. *IEEE Transactions on Antennas and Propagation*, 2012, vol. 60, no. 10, p. 4677–4687. DOI: 10.1109/TAP.2012.2207030

[7] ZHANG, H., ZHOU, P., LU, H., et al. Resistance selection of high impedance surface absorbers for perfect and broadband absorption. *IEEE Transactions on Antennas and Propagation*, 2013, vol. 61, no. 2, p. 976–979. DOI: 10.1109/TAP.2012.2226225

[8] PANG, Y., CHENG, H., ZHOU, Y., WANG, J. Analysis and enhancement of the bandwidth of ultrathin absorbers based on high-impedance surfaces. *Journal of Physics D: Applied Physics*, 2012, vol. 45, no. 21, p. 215104 (5 p.). DOI: 10.1088/0022-3727

[9] SUN, W., HE, Q., HAO, J., ZHOU, L. A transparent metamaterial to manipulate electromagnetic wave polarizations. *Optics Letters*, 2011, vol. 36, no. 6, p. 927–929. DOI: 10.1364/OL.36.000927

[10] HAO, J., YUAN, Y., RAN, L., et al. Manipulating electromagnetic wave polarizations by anisotropic metamaterials. *Physical Review*

*Letters*, 2007, vol. 99, no. 6, p. 063908-(1–4). DOI: 10.1103/PhysRevLett.99.063908

[11] RAJKUMAR, R., YOGESH, N., SUBRAMANIAN, V. Cross polarization converter formed by rotated-arm-square chiral metamaterial. *Journal of Applied Physics*, 2013, vol. 114, no. 22, p. 224506-(1–7). DOI: 10.1063/1.4846096

[12] KHANIKAEV, A. B., MOUSAVI, S. H., WU, C., et al. Electromagnetically induced polarization conversion. *Optics Communications*, 2012, vol. 285, p. 3423–3427. DOI: 10.1016/j.optcom.2012.03.023

[13] CHENG, Y., NIE, Y., GONG, R. A polarization-insensitive and omnidirectional broadband terahertz metamaterial absorber based on coplanar multi-squares films. *Optics and Laser Technology*, 2013, vol. 48, p. 415–421. DOI: j.optlastec.2012.11.016

[14] LI, S., GAO, J., CAO, X., et al. Wideband, thin, and polarization-insensitive perfect absorber based the double octagonal rings metamaterials and lumped resistances. *Journal of Applied Physics*, 2014, vol. 116, no. 4, p. 043710-(1–6). DOI: 10.1063/1.4891716

[15] GRANT, J., MA, Y., SAHA, S., et al. Polarization insensitive terahertz metamaterial absorber. *Optics Letters*, 2011, vol. 36, no. 8, p. 1524–1526. DOI: 10.1364/OL.36.001524

[16] LI, S. J., GAO, J., CAO, X. Y., et al.Multiband and broadband polarization-insensitive perfect absorber devices based on a tunable and thin double split-ring metamaterial. *Optics Express*, 2015, vol. 23, no. 3, p. 3523–3533. DOI: 10.1364/OE.23. 003523

[17] LI, S. J., GAO, J., CAO, X. Y., et al. Polarization-insensitive and thin stereometamaterial with broadband angular absorption for oblique incidence. *Applied Physics A*, 2015, vol. 119, no. 1, p. 371–378. DOI: 10.1007/s00339-014-8978-y

[18] WU, L., YANG, Z., CHENG, Y., et al. Giant asymmetric transmission of circular polarization in layer-by-layer chiral metamaterials. *Applied Physics Letters*, 2013, vol. 103, no. 2, p. 021903-(1–4). DOI: 10.1063/1.4813487

[19] SHI, J., LIU, X., YU, S., et al. Dual-band asymmetric transmission of linear polarization in bilayered chiral metamaterial. *Applied Physics Letters*, 2013, vol. 102, no. 19, p. 191905-(1–5). DOI: 10.1063/1.4805075

[20] ZHU, W., RUKHLENKO, I. D., XIAO, F., PREMARATNE, M. Polarization conversion in U-shaped chiral metamaterial with four-fold symmetry breaking. *Journal of Applied Physics*, 2014, vol. 115, p. 143101-(1–4). DOI: 10.1063/1.4870862

[21] JIA, Y., ZHANG, Y., DONG, X., et al. Complementary chiral metasurface with strong broadband optical activity and enhanced transmission. *Applied Physics Letters*, 2014, vol. 104, no. 1, p. 011108-(1–5). DOI: 10.1063/1.4861422

[22] MUTLU, M., AKOSMAN, A. E., SEREBRYANNIKOV, A. E., OZBAY, E. Asymmetric chiral metamaterial circular polarizer based on four U-shaped split ring resonators. *Optics Letters*, 2011, vol. 36, no. 9, p. 1653–1655. DOI: 10.1364/OL.36.001653.

[23] YAN, S., VANDENBOSCH, G. A. E. Compact circular polarizer based on chiral twisted double split-ring resonator. *Applied Physics Letters*, 2013, vol. 102, no. 10, p. 103503. DOI: 10.1063/1.4794940

[24] XU, H., WANG, G., QI, M., et al. Compact dual-band circular polarizer using twisted Hilbert-shaped chiral metamaterial. *Optics Express*, 2013, vol. 21, no. 21, p. 024912. DOI: 10.1364/OE.21.024912

[25] MA, X., HUANG, C., PU, M., et al. Multi-band circular polarizer using planar spiral metamaterial structure. *Optics Express*, 2012, vol. 20, no. 14, p. 016050–016058. DOI: 10.1364/OE.20.016050

[26] SHEN, N., ZHANG, L., KOSCHNY, T., et al. Discontinuous design of negative index metamaterials based on mode hybridization. *Applied Physics Letters*, 2012, vol. 101, no. 8, p. 081913-(1–3). DOI: 10.1063/1.4748361

[27] LI, Z., ZHAO, R., KOSCHNY, T., et al. Chiral metamaterials with negative refractive index based on four U split ring resonators. *Applied Physics Letters*, 2010, vol. 97, no. 8, p. 081901-(1–3). DOI: 10.1063/1.3457448

[28] SHEN, N., KOSCHNY, T., KAFESAKI, M., SOUKOULIS, C. M. Robust wedge demonstration to optical negative index metamaterials. *Applied Physics Letters*, 2013, vol. 102, no. 24, p. 241915-(1–4). DOI: 10.1063/1.4812240

[29] EKMEKCI, E., TURHAN-SAYAN G. Multi-functional metamaterial sensor based on a broad-side coupled SRR topology with a multi-layer substrate. *Applied Physics A*, 2013, vol. 110, no. 1, p. 189–197. DOI: 10.1007/s00339-012-7113-1

[30] MA, H., TANG, W., CHENG, Q., CUI, T. A single metamaterial plate as bandpass filter, transparent wall, and polarization converter controlled by polarizations. *Applied Physics Letters*, 2014, vol. 105, no. 8, p. 081908-(1–5). DOI: 10.1063/1.4894370

[31] SHI, H., LI, J., ZHANG, A., et al. Broadband cross polarization converter using plasmon hybridizations in a ring/disk cavity. *Optics Express*, 2014, vol. 22, no. 17, p. 20973–20981. DOI: 10.1364/OE.22.020973

[32] STUTZMAN, W. L., THIELE, G. A. *Antenna Theory and Design*. 2nd ed. Wiley Publishing, 1998. ISBN: 0471025909

[33] CHENG, Y., WITHAYACHUMNANKUL, W., UPADHYAY, A., et al. Ultrabroadband reflective polarization convertor for terahertz waves. *Applied Physics Letters*, 2014, vol. 105, no. 18, p. 181111-(1–4). DOI: 10.1063/1.4901272

[34] SHI, H., ZHANG, A., ZHENG, S., et al. Dual-band polarization angle independent 90° polarization rotator using twisted electric-field-coupled resonators. *Applied Physics Letters*, 2014, vol. 104, no. 3, p. 034102-(1–4). DOI: 10.1063/1.4863227

## About the Authors ...

**Zhao ZHANG** was born in Baoji, Shaanxi province, China in 1990. He received B.S. and M.S. from the Air Force Engineering University, Xi'an China, in 2012 and 2014. He is currently working toward Ph.D. degree at the Information and Navigation College, Air Force Engineering University. His main interests include titled beam antennas, circularly polarized antennas, metamaterial design and RCS reduction.

**Xiangyu CAO** received the B.Sc and M.A.Sc degrees from the Air Force Missile Institute in 1986 and 1989, respectively. She joined the Air Force Missile Institute in 1989 as an assistant teacher. She became an associate professor in 1996. She received Ph.D. degree in the Missile Institute of Air Force Engineering University in 1999. From 1999 to 2002, she was engaged in postdoctoral research in Xidian University, China. She was a Senior Research Associate in the Department of Electronic Engineering, City University of Hong Kong from Jun. 2002 to Dec. 2003. She is currently a professor of the Air Force Engineering University of CPLA. Her research interests include computational electromagnetic, smart antennas, electromagnetic metamaterial and their antenna applications, and electromagnetic compatibility.